Analysis of Electromagnetic Waves from Shadow Regions of Conducting Cylinders with Wedge Cavities

[#]Shinichiro Ohnuki[1], Shuichi Shinohara[1], Ryuichi Ohsawa[2], Tsuneki Yamasaki[1]
[1]Department of Electrical Engineering, College of Science and Technology, Nihon University
1-8-14 Surugadai, Kanda, Chiyoda-ku, Tokyo, 101-8308, Japan
E-mail: ohnuki.shinichiro@nihon-u.ac.jp
[2]MITSUMI Electric Co.,Ltd.
2-33-2,Tsurumaki,Tama-shi,Tokyo,206-8567 Japan

Abstract

High precision analysis of electromagnetic scattering problems for conducting cylinders with wedge cavities is performed. Contribution of electromagnetic waves from shadow regions is clarified for varying the shapes of cavities.

Keywords : electromagnetic scattering wedge cavities point matching method

1. Introduction

Analysis of electromagnetic scattering is important for target recognition and reduction of the radar cross section (RCS) [1,2]. When targets have concave or convex portions has a cavity, the scattering phenomena become more complicated due to the multiple scattering and resonance inside the cavity [3]. Hence, development of a highly reliable computational technique is important. The authors have proposed a kind of mode matching techniques, the point matching method (PMM) taking into account of the edge conditions, and reported that electromagnetic scattering problems can be analyzed with high accuracy [4-6]. In this paper, high precision analysis of electromagnetic scattering problems is performed by using our proposed technique and contribution of electromagnetic waves from shadow regions of conducting cylinders with deep wedge cavities is clarified.

2. Formulation

A scatterer shown in Fig. 1 is assumed to be uniform along the *z*-axis. The original structure is the rectangular cylinder whose cross section is 2*a*×2*b*. Here, *P* is the intersection point on the bottom plate. The cavity is formed to shift the midpoint of the side of a rectangle along the *x*-axis.

In our PMM, the whole physical space is divided into a finite number of sub-domains in which electromagnetic fields can be expanded by a sum of solutions to the Helmholtz equation. Considering the symmetry along the *x*-axis, we introduce the field decompositions in the upper half-space $(y \geq 0)$. The following seven regions shown in Fig. 2 are introduced.

Region S_0 : Outside the circle C_0 [origin O , radius ρ_0]

The scattered field in this region satisfies the radiation condition. Therefore it can be approximated using a finite sum of modes in the coordinates

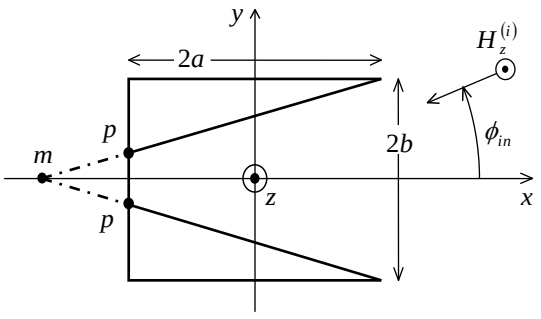

Figure 1: Geometry of a conducting rectangular cylinder with a deep wedge cavity.

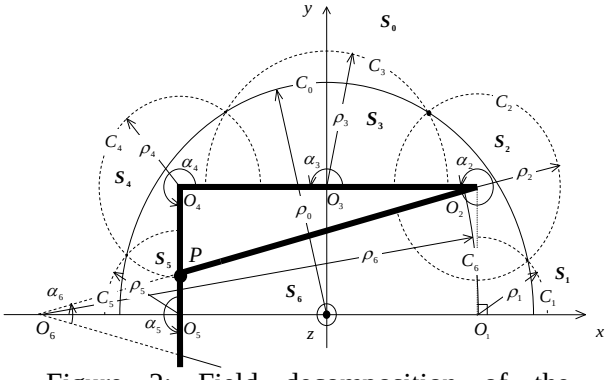

Figure 2: Field decomposition of the physical space for the PMM.

$$H_z^{(S_0)}[p]=\sum_{n=p}^{N-1}A_n[p]\,H_n^{(2)}(kr)\cos\left(n\theta-\frac{\pi}{2}p\right), \tag{1}$$

where $\rho_0 := (1+\delta)\sqrt{a^2+b^2}$, $H_n^{(2)}(\cdot)$ is the $n-$th order of the second kind of the Henkel function, $A_n[p]$ is unknown for the even phase $(p=0)$ and the odd phase $(p=1)$, and N is the truncation number.

Region S_1: Inside the circle C_1 [origin O_1, radius ρ_1]

This region is adjacent to the open-ended of the cavity. Therefore the field can be expanded by using the combination of trigonometric function, such as

$$H_z^{(S_1)}[p]=\sum_{n=p}^{M_1-1}J_n(kr_1)\left\{(1-p)B_n^{(1)}[0]\cos(n\theta_1)+pB_n^{(1)}[1]\sin(n\theta_1)\right\}, \tag{2}$$

where $\rho_0 := (1+\delta)\sqrt{a^2+b^2}$, $J_n(\cdot)$ is the $n-$th order of the Bessel function, $B_n[p]$ is unknown, M_1 is the truncation number, and $m=2n+p$.

Region S_l: Inside the circle C_l $(l=2-5)$[origin O_l, radius ρ_l]

To satisfy the edge condition, the magnetic field can be written in the local coordinate system as

$$H_z^{(S_l)}[p]=\sum_{n=0}^{M_l-1}B_n^{(l)}[p]\,J_{\nu_l n}(kr_l)\cos(\nu_l n\theta_l), \tag{3}$$

where $J_{\nu_l}(\cdot)$ is the ν_l-th order of the Bessel function, M_l is the truncation mode number for each separated region, and $\nu_l=\pi/\alpha_l$, $m=2n+p$ for $l=5$ and $m=n$ for $l=2-4$.

Region S_6: Inside the circle C_6 [origin O_6, radius ρ_6]

The field can be expanded using the combination of the ν_6-th order of the Bessel and Neumann functions as follows;

$$H_z^{(S_6)}[p]=\sum_{n=0}^{M_6-1}B_n^{(6)}[p]\left\{\,J_{\nu_6(2n+p)}(kr_6)+D_{(2n+p)}N_{\nu_6(2n+p)}(kr_6)\,\right\}\cos\{\nu_6(2n+p)\theta_6\}, \tag{4}$$

where $D_n=-J'_{\nu 6n}(kd)/N'_{\nu 6n}(kd)$, $\nu_6=\pi/\alpha_6$, and kd is the distance $\overline{O_6P}$.

The unknown expansion coefficients are determined to satisfy the continuity conditions at the sampling point which are placed at the almost same interval on the boundaries [5].

3. Computational Results

The RCS is investigated when a plane *H*-wave is incident on the scatterer from $\phi_{in}=180°$ when $\alpha_1=90°, \alpha_3=\alpha_5=180°$, and $\alpha_4=270°$. These parameters are fixed hereafter. Fig. 3 shows the bistatic RCS when the size of the scatterer is $ka=47.1$. The solid line shows the computational result for $\alpha_2=360°$ $(\alpha_6=0°)$ and dots show that for $\alpha_2=356°$ $(\alpha_6=8°)$. We cannot distinguish these results at almost all the observation angles, since the shapes of the illuminated regions are the same flat plate for the both cases. To study contribution of electromagnetic waves from the shadow region, the difference D_σ and $\overline{D_\sigma}$ between two RCSs are defined as follows:

$$D_\sigma(\theta)=\frac{\left|(\sigma/\lambda)_{\alpha_2=356°}-(\sigma/\lambda)_{\alpha_2=360°}\right|}{\max\left[(\sigma/\lambda)_{\alpha_2=360°}\right]}$$

$$\overline{D_\sigma}(\theta)=\frac{1}{2P}\sum_{n=-P}^{P-1}D_\sigma(\theta+n\Delta\theta)$$

$$\Delta\theta=\frac{2\pi}{P_t} \tag{5}$$

where max[ζ] is the maximum value of ζ, P_t is the total number of observation angles, and P is the number of samples near θ for taking the average. For the observation angle θ, D_σ and $\overline{D_\sigma}$ with $P_t=3{,}600$ and $P=100$ are plotted in Fig. 4. The difference $\overline{D_\sigma}$ of the RCSs for $\alpha_2=356°$ and $\alpha_2=360°$ appears in the fourth digit for observation angles $|\theta|\le 80°$ $(D_\sigma\cong\overline{D_\sigma}\cong 10^{-4})$ and in the fifth digit of the RCS for observation angles $|\theta|\ge 80°$ $(D_\sigma\cong\overline{D_\sigma}\cong 10^{-5})$.

Figs. 5 and 6 show the RCSs of $ka = 3.14$ and $ka = 3.51$, respectively. Other parameters are the same as the case in Fig. 3. Differences can be recognized at observation angles around $\theta = 90°$ when $ka = 3.14$. On the other hand, differences for $ka = 3.51$ can be observed at all the observation angles. Fig. 7 shows $\overline{D_\sigma}$ for the both cases. In the case of $ka = 3.51$, the angular dependence is smaller in comparison with the case of $ka = 3.14$ and the difference becomes $\overline{D_\sigma} \cong 10^{-1}$ at all the observation angles. To study the field distribution when $ka = 3.51$, we plot the magnetic field inside and outside cavities for $\alpha_2 = 360°$ and $\alpha_2 = 356°$ in Figs. 8 and 9, respectively. Difference of the field distribution can be easily recognized, since the cavity resonance is observed when $\alpha_2 = 356°$.

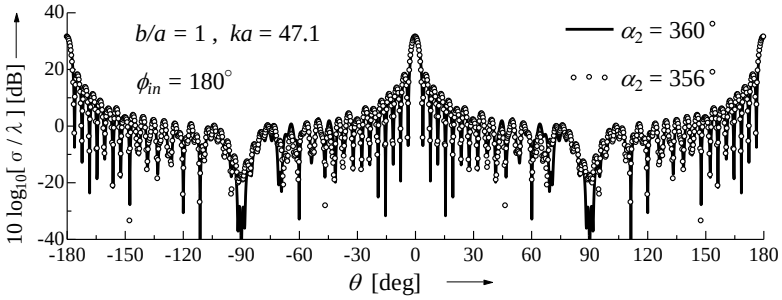

Figure 3: Bistatic RCS for $ka = 47.1$.

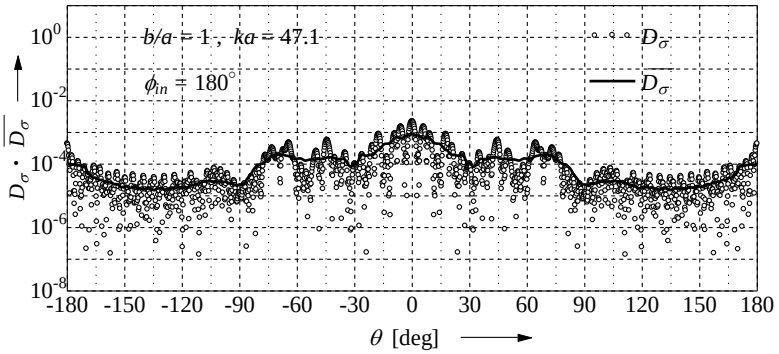

Figure 4: Difference between two RCSs for $ka = 47.1$.

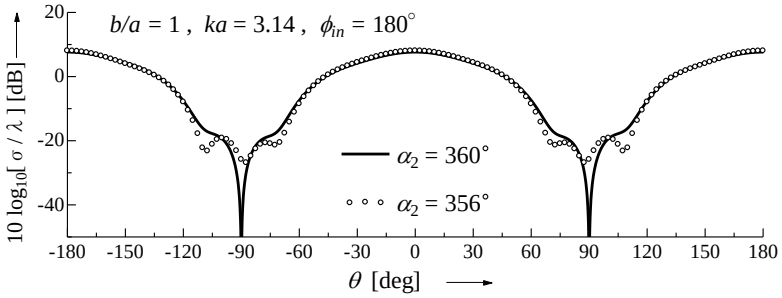

Figure 5: Bistatic RCS for $ka = 3.14$.

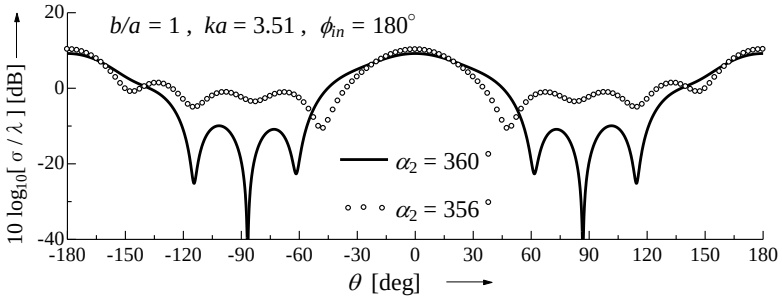

Figure 6: Bistatic RCS for $ka = 3.51$.

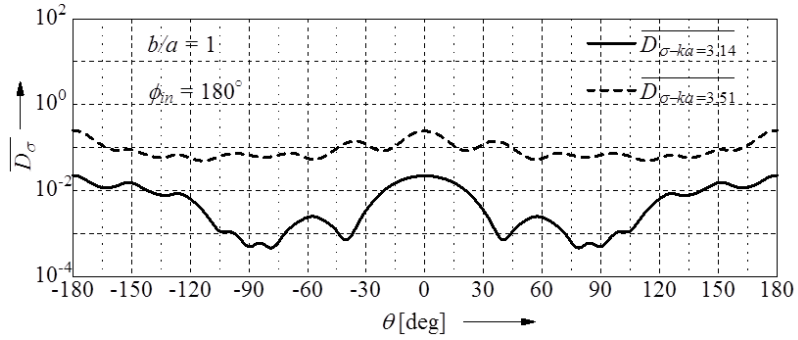

Figure 7: Comparison between two $\overline{D_\sigma}$ for $ka = 3.14$ and $ka = 3.51$.

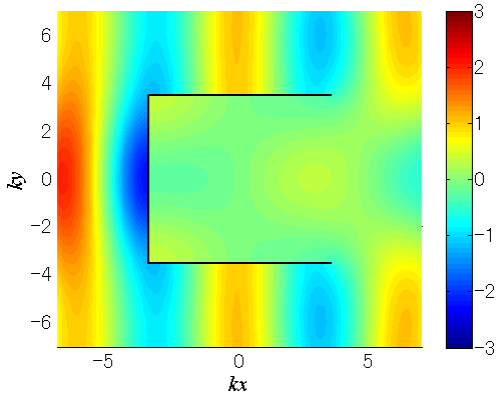

Figure 8: Magnetic field of the wedge cavity for $\alpha_2 = 360°$ and $ka = 3.51$.

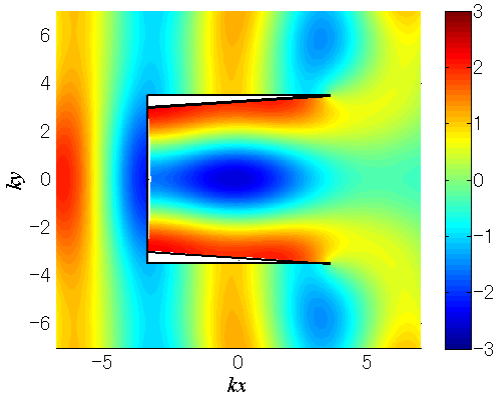

Figure 9: Magnetic field of the wedge cavity for $\alpha_2 = 356°$ and $ka = 3.51$.

4. Conclusions

In this paper, we study electromagnetic scattering from conducting rectangular cylinders with deep wedge cavities by using a king of mode matching technique. Contribution of electromagnetic waves from the shadow region is clarified.

References

[1] E. F.Knott, J. F.Shaeffer, and M. T. Tuley, Radar Cross Section: Second Edition, Artech House, 1993.

[2] A. K. Bhattacharyya, High-frequency electromagnetic techniques Recent advances and applications, John Wiley & Sons, 1995.

[3] M. Hashimoto, "Locations of Zeros for Electromagnetic Fields Scattered by Polygonal Objects," IEICE Trans. Electron., vol. E87-C, no. 9, pp. 1595-1606, 2004.

[4] T. Yamasaki, T. Hinata, and T. Hosono, "Scattering of plane electromagnetic waves by a conducting rectangular cylinder: Point matching method considering edge condition," IEICE Trans. C-I, vol. J72-C-I, no. 11, pp. 703-710, 1989 (in Japanese).

[5] S. Ohnuki and T. Hinata, "RCS of material partially loaded parallel plate waveguide cavities, "IEEE Trans. Antennas Propagat., vol. 51, no. 2, pp. 337-344, February 2003.

[6] S. Ohnuki, R. Ohsawa, and T. Yamasaki, "Electromagnetic Scattering from Rectangular Cylinders with Various Wedge Cavities and Bumps," IEICE Trans. Electron., vol. E93-C, no. 1, pp. 77-80, 2010.

Acknowledgments

The authors are grateful to Yohei Sekiguchi for carrying out some of the computations. This work was partly supported by Nihon University Strategic Projects for Academic Research.